

Low-cost synthesis of α -Fe₂O₃ nanorods for photocatalytic application

Hoai Nhan Luong^{1,2}, Le Ngoc Thu Nguyen^{1,2}, Tan Muon Dinh^{1,2}, Nguyen Dan Nhi Huynh^{1,2}, Le Thai Duy^{1,2}, Cong Khanh Tran^{1,2}, Vinh Quang Dang^{1,2,*}



Use your smartphone to scan this QR code and download this article

ABSTRACT

Introduction: α -Fe₂O₃ nanorods (α -Fe₂O₃ NRs), also known as hematite, possess a narrow band gap, high chemical stability, extensive surface area, controllable size, and outstanding photoelectric properties. These attributes make hematite a promising material for various applications, including gas sensors, optical sensors, and notably, photocatalysis. In previous studies, α -Fe₂O₃ nanorods were synthesized using various processes. However, these processes involve extensive use of precursors, are expensive, and time-consuming, and have negative impacts on the environment. Hence, this investigation introduces an uncomplicated, efficient, and high-precision hydrothermal process for synthesizing α -Fe₂O₃ nanorods (α -Fe₂O₃ NRs). **Methods:** We utilized a short-term hydrothermal process to synthesize α -Fe₂O₃ nanorods. Characterization of the nanorods involved XRD, VESTA, Raman, SEM, and EDX to examine their morphology and structure, with UV-Vis spectroscopy used to determine their absorption spectra. The photocatalytic efficiency of the α -Fe₂O₃ nanorods was assessed by their ability to degrade methylene blue dye at a concentration of 2.5 ppm. **Results:** VESTA simulations and XRD patterns confirmed that the α -Fe₂O₃ nanorods have a rhombohedral crystal structure and belongs to space group $R\bar{3}c$. The optical bandgap was determined to be 2.2 eV through calculations using Tauc's method. Through scanning electron microscopy (SEM), the average length and diameter of the α -Fe₂O₃ NRs were determined to be 415 nm and 110 nm, respectively. The photocatalytic capacity for degrading methylene blue (concentration of 2.5 ppm) was 55%. **Conclusion:** This exploration of the fundamental characteristics of α -Fe₂O₃ NRs offers deeper insights into the properties of nanorod-structured hematite materials. Moreover, the synthesis of α -Fe₂O₃ NRs using this hydrothermal method addresses several previously identified challenges, thereby contributing to broadening the potential applications of α -Fe₂O₃ NRs across various fields in the future.

Key words: α -Fe₂O₃ nanorods, hematite, photocatalyst, VESTA, simulation

¹Faculty of Materials Science and Technology, University of Science, Ho Chi Minh City, Vietnam

²Vietnam National University, Ho Chi Minh City, Vietnam

Correspondence

Vinh Quang Dang, Faculty of Materials Science and Technology, University of Science, Ho Chi Minh City, Vietnam

Vietnam National University, Ho Chi Minh City, Vietnam

Email: vinhquangntmk@gmail.com

History

- Received: 2024-03-30
- Accepted: 2024-05-31
- Published Online: 2024-6-xx

DOI :



Copyright

© VNUHCM Press. This is an open-access article distributed under the terms of the Creative Commons Attribution 4.0 International license.



1 INTRODUCTION

2 In recent decades, the synthesis of one-dimensional
3 (1D) nanostructures has garnered significant atten-
4 tion and extensive research across various fields
5 due to their unique physical and chemical prop-
6 erties¹. Additionally, the morphological diversity
7 of one-dimensional nanostructures offers numerous
8 advantages for various applications. For example,
9 nanowires possess a high surface area-to-volume ra-
10 tio, low defect density, and excellent optical conduc-
11 tivity, making them suitable for various applications,
12 such as nanobiosensors, chemical sensors, gas sen-
13 sors, and electrochemical sensors². Due to their high
14 specific surface area, nanotube structures can serve as
15 frameworks or containers for other materials that can
16 be applied in fuel cells, photocatalytic systems, energy
17 storage, gas sensors, etc.,³. One particularly special
18 and easily fabricated form of the 1D nanostructure
19 is nanorods, which are characterized by large surface

20 areas, easily controllable dimensions, and excellent
21 optoelectronic properties. Nanorods have numer-
22 ous important applications in light-emitting diodes
23 (LEDs), light sensors, photocatalysis, gas sensors,
24 biosensors, etc.⁴ Among the various types of 1D ma-
25 terials, α -Fe₂O₃ nanorods, also known as hematite,
26 stand out due to their narrow band gap (approx-
27 imately 2.2 eV), chemical stability, and nontoxic na-
28 ture⁵. This makes hematite a highly significant ma-
29 terial in numerous fields, such as magnetic applica-
30 tions^{6,7}, gas sensors⁸, lithium-ion batteries⁹, drug
31 delivery technology¹⁰, and particularly photocataly-
32 sis¹¹⁻¹⁴. α -Fe₂O₃ nanorods have been synthesized
33 using various physical and chemical methods, such
34 as sol-gel methods¹⁵, hydrothermal methods¹⁶, vac-
35 uum thermal evaporation methods¹⁷, green chem-
36 istry methods¹⁸, and micelle methods¹⁹. However,
37 physical methods often require expensive equipment
38 and complex procedures, leading to limitations in

Cite this article : Luong H N, Nguyen L N T, Dinh T M, Huynh N D N, Duy L T, Tran C K, Dang V Q. **Low-cost synthesis of α -Fe₂O₃ nanorods for photocatalytic application.** *Sci. Tech. Dev. J.* 2024; 27():1-10.

39 practical applications hence, chemical methods are
40 usually preferred. Among them, the hydrothermal
41 method has become the preferred choice for α -Fe₂O₃
42 nanorod synthesis due to its low cost, simple synthesis
43 process, and high efficiency compared to other meth-
44 ods. Despite its numerous advantages, hydrothermal
45 synthesis still faces some challenges due to the use
46 of multiple toxic precursors and prolonged reaction
47 times, which can have negative environmental im-
48 pacts. This can be observed in some previous studies.
49 For instance, *Gajendra and colleagues* conducted a hy-
50 drothermal process for up to 36 hours, with an addi-
51 tional 3 hours required to obtain α -Fe₂O₃ nanorods
52 using precursors such as diammonium phosphate and
53 iron (III) chloride hexahydrate²⁰. Additionally, the
54 research group led by *Suyuan Zeng* synthesized α -
55 Fe₂O₃ nanorods using a hydrothermal method with
56 a total reaction time of 20 hours, employing sodium
57 sulfite and iron(II) sulfate as precursors²¹. Further-
58 more, by utilizing iron(III) nitrate nonahydrate and
59 sodium hydroxide for a 12-hour hydrothermal pro-
60 cess, *Guo-Ying Zhang and colleagues* successfully syn-
61 thesized α -Fe₂O₃ nanorods for photocatalytic appli-
62 cations²².

63 In addition to the challenges related to the use
64 of multiple precursors and long synthesis times,
65 most research on photocatalysis only utilizes α -
66 Fe₂O₃ nanorods (NRs) as a supporting material com-
67 bined with other substances, such as cadmium oxide
68 nanoparticles¹², cadmium sulfide nanoparticles²³,
69 chromium dopants¹³, or hybridization with reduced
70 graphene oxide (rGO)²⁴. This inadvertently blurs the
71 distinctive properties of α -Fe₂O₃ NRs in photocal-
72 ysis, significantly impacting the optimization and en-
73 hancement of material structures to achieve maxi-
74 mum performance for future studies. Therefore, in
75 this study, we focused on developing a simple hy-
76 drothermal process that saves time and utilizes fewer
77 precursors to synthesize α -Fe₂O₃ nanorods. Addi-
78 tionally, the properties of the hematite material are ex-
79 amined and clearly presented through a combination
80 of experimental work and simulation calculations.
81 Furthermore, the photocatalytic capability of the α -
82 Fe₂O₃ NRs was investigated through the degrada-
83 tion of methylene blue (MB) dye. With this method,
84 this study not only provides a clearer understanding
85 of the material but also partially addresses some of
86 the abovementioned challenges, thereby contributing
87 to expanding the potential applications of α -Fe₂O₃
88 nanorods in various fields in the future, both gener-
89 ally and particularly in the field of photocatalysis.

MATERIALS-METHODS

Chemical materials

The chemicals used in this experiment included
iron(III) chloride hexahydrate (FeCl₃·6H₂O, 99%,
SigmaAldrich, USA), sodium nitrate (NaNO₃, 99%,
SigmaAldrich, USA), and methylene blue (82%, Sig-
maAldrich, USA).

Characteristics

The surface morphology and density of the nanorods
were examined using scanning electron microscopy
(SEM, Hitachi S-4800). The crystalline structure
of the α -Fe₂O₃ nanorods was observed via X-ray
diffraction (XRD) performed on a D8 Advance-
Bruker X-ray diffractometer operating at 40 kV and
100 mA with a Cu/K α radiation source ($\lambda = 0.154$
nm). The optical properties of the nanorods were
determined through UV-Vis spectroscopy (JASCO
V670). Raman spectra were recorded using a Raman
spectrometer (Xplora One, HORIBA) with an excita-
tion wavelength of 532 nm, a power of 5 mW, a 10 \times
objective, and an acquisition time adjusted to 15 sec-
onds per spectrum. 3D structural models and XRD
patterns based on computational simulations of α -
Fe₂O₃ nanorods were generated using VESTA soft-
ware (Visualization for Electronic Structural Analy-
sis).

The photocatalytic efficiency of the α -Fe₂O₃
nanorods (NRs) was assessed by their ability to
degrade methylene blue (MB) dye. The sample,
with a size of 2 cm \times 2 cm of α -Fe₂O₃ thin film,
was added to 20 mL of the 2.5 ppm MB solution
and then stirred evenly in the dark for 2 hours to
ensure adsorption equilibrium. Subsequently, the
sample was irradiated under visible light for 8 hours.
The illumination source was a visible light lamp,
equivalent to 1 sun, and a cooling fan was utilized to
maintain the ambient temperature. The absorbance
spectra of the MB solution were recorded at 2-hour
intervals.

Fabrication processes

The synthesis of the α -Fe₂O₃ nanorods followed a
hydrothermal method similar to that used in *Dong*
Chen's study²⁵. Initially, a solution containing
FeCl₃·6H₂O (0.15 M) and NaNO₃ (1 M) with a to-
tal volume of 10 mL was prepared at room tempera-
ture. Once the precursors were completely dissolved
in the solution, the mixture was transferred to a 25
mL Teflon-lined autoclave. Subsequently, a clean sil-
icon substrate was placed inside the autoclave, which
was then placed in an oven at 100 °C for 4 hours to

form FeOOH nanorods. Next, the sample was washed multiple times with deionized water and ethanol to remove impurities. Finally, the FeOOH sample was transferred to a furnace and annealed at 550 °C for 2 hours to convert it into α -Fe₂O₃ nanorods.

RESULTS

The simulated structure of α -Fe₂O₃ is depicted in Figure 1. Hematite possesses a rhombohedral crystal structure and belongs to the space group $R\bar{3}c$ ²⁶. In each primitive cell, there are two formula units ($a_{rh} = 5.427$ Å; $a = 55.3$) (Figure 1a), whereas the unit cell contains six formula units ($a = b = 5.034$ Å; $c = 13.75$ Å) (Figure 1b)²⁷. Furthermore, the arrangement of anions and cations results in an octahedral structure comprising one iron atom and six oxygen atoms (Figure 1c).

X-ray diffraction (XRD) patterns obtained experimentally and through simulation were utilized to evaluate the crystal structure of α -Fe₂O₃, as shown in Figure 2. There are 14 characteristic diffraction peaks of α -Fe₂O₃ obtained experimentally at 2θ angles of 24°, 32°, 35°, 39°, 40°, 43°, 49°, 53°, 57°, 61°, 63°, 69°, 71°, and 74° corresponding to lattice planes (012), (104), (110), (006), (113), (202), (024), (116), (018), (214), (300), (208), (119), and (217), respectively. These peaks coincide with the simulated diffraction peaks and are all in good agreement with JCPDS number 33-0664²⁸.

The optical properties of α -Fe₂O₃ are illustrated in Figure 3, which shows the light absorption of our sample in the wavelength range from 380 nm to 1000 nm. Clearly, the absorption peak is found ca. 400 nm (Figure 3a). A further analysis using Tauc's plot (Figure 3b) revealed that the optical bandgap of our iron oxide material was approximately 2.2 eV, which is similar to the band gap values of α -Fe₂O₃ in other reports²⁹. Additionally, the bandgap energy (E_g) is calculated to be approximately 2.2 eV using the Kubelka-Munk equation³⁰:

$$(\alpha hv)^n = A (hv - E_g)$$

where A is a constant, hv is the intensity of the incident light, α is the absorption coefficient, and n is 1/2 for the indirect bandgap and 2 for the direct bandgap.

Figure 4a-c displays SEM images of α -Fe₂O₃ nanorods synthesized at different hydrothermal times (3 h, 4 h, and 5 h). At a hydrothermal duration of 3 hours, the nanorods are still in the early stages of development, exhibiting a fragmented distribution. Conversely, the samples treated for 4 and 5 hours had nanorods with consistent density and well-defined

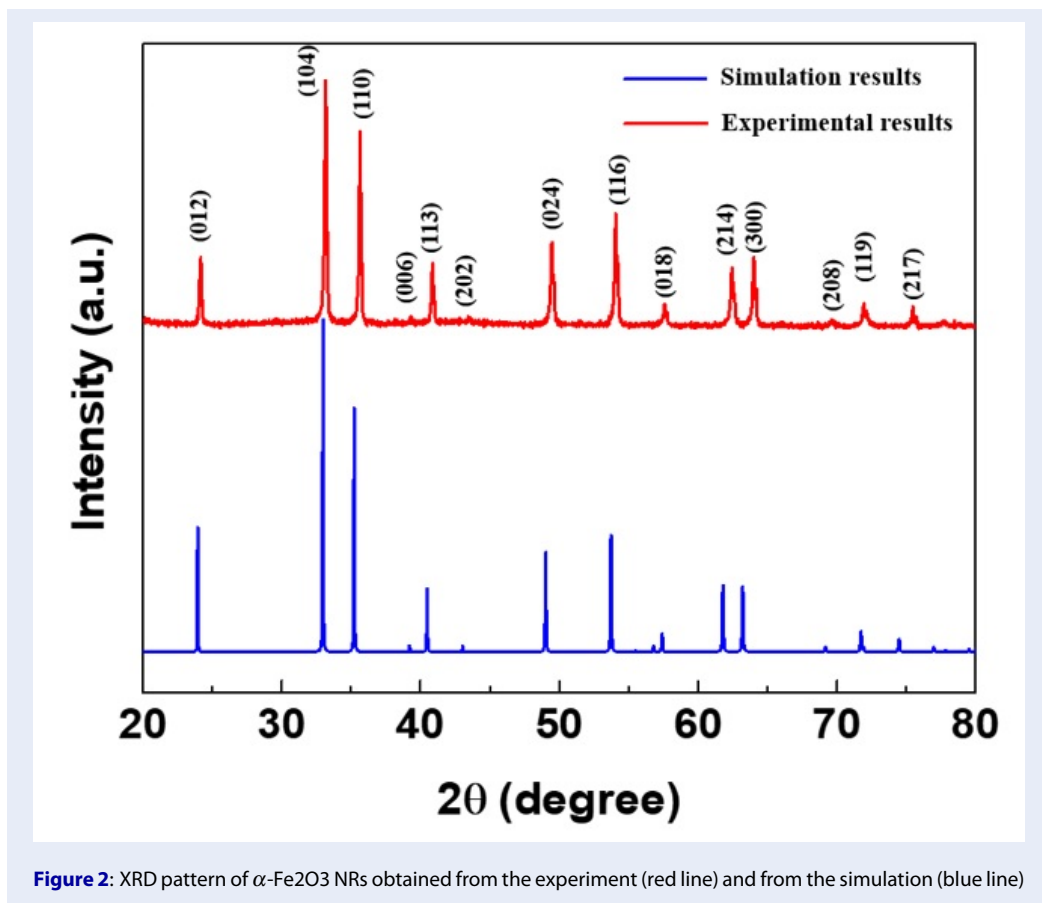
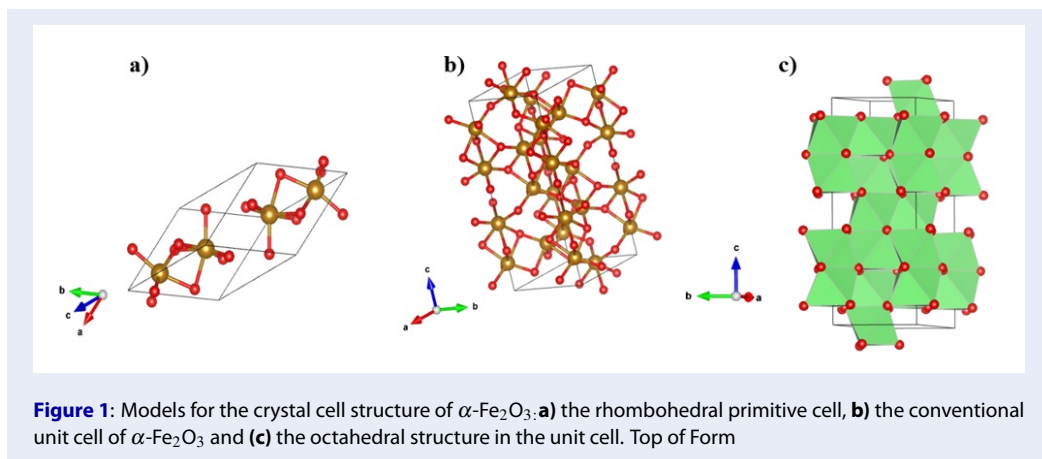
structures. However, considering the time and energy efficiency, the 4-hour hydrothermal sample was selected as the most suitable sample for further investigation. Subsequently, SEM analysis at a scale of 1 μ m (Figure 4d) revealed uniform growth of nanorods across a substantial area. Additionally, EDX analysis (Figure 4e) detected Fe, O, Si, and C elements without any presence of any foreign elements, further confirming the high purity of the synthesized sample.

Figure 5 shows the Raman spectrum of the α -Fe₂O₃ nanorods. Apart from the characteristic peak of the silicon substrate at 521 cm⁻¹, the remaining peaks are indicative of the hematite structure^{31,32}. Specifically, the peaks at 224 and 475 cm⁻¹ are assigned to the A_{1g} vibrational mode, while the five peaks at approximately 244, 291, 408, 609, and 814 cm⁻¹ are attributed to the E_g mode.

Figure 6a and Figure 6b depict the absorption spectra of the MB solution in the absence and presence of α -Fe₂O₃ NRs under visible light, respectively. Throughout the dark stirring process, the maximum absorption intensity of the MB solution containing the α -Fe₂O₃ NRs gradually decreased, indicating that MB adsorbed onto the stable material surface. Upon illumination, the intensity of the absorption peak of the MB solution with the α -Fe₂O₃ NRs catalyst decreased more rapidly over time than that of the solution without the catalyst. This observation proves that the α -Fe₂O₃ NRs material exhibits photocatalytic activity in the visible light region. Hence, to further assess the photocatalytic performance, the degradation efficiency and reaction rate constant of MB by the α -Fe₂O₃ NRs were calculated (Figure 7).

DISCUSSION

The VESTA simulation findings for the crystal structure of α -Fe₂O₃ (Figure 1) reveal that the hematite structure is based on the arrangement of O²⁻ anions, which form a hexagonal close-packed (HCP) lattice along the [001] direction of the Fe³⁺ cations. One iron atom and six oxygen atoms form an octahedral unit, with each octahedral unit sharing edges with three neighboring octahedra in the same plane. Consequently, the octahedral units undergo distortion, resulting in two different bond lengths of Fe-O, measured at 1.98 Å and 2.09 Å³³. In the XRD pattern (Figure 2), the experimentally synthesized sample exhibits the presence of 14 characteristic diffraction peaks of α -Fe₂O₃ without any additional peaks, indicating the high purity of the sample obtained through the hydrothermal method in this study. This finding contributes to demonstrating the successful attainment of



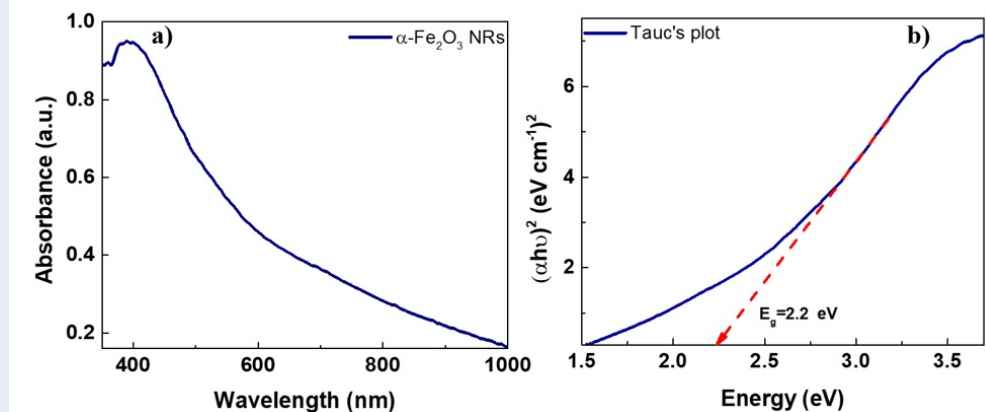


Figure 3: a) UV-Vis absorption spectrum was recorded from the wavelength of 350 to 1000 nm and b) The optical bandgap of the α -Fe₂O₃ NRs was calculated from Tauc's method

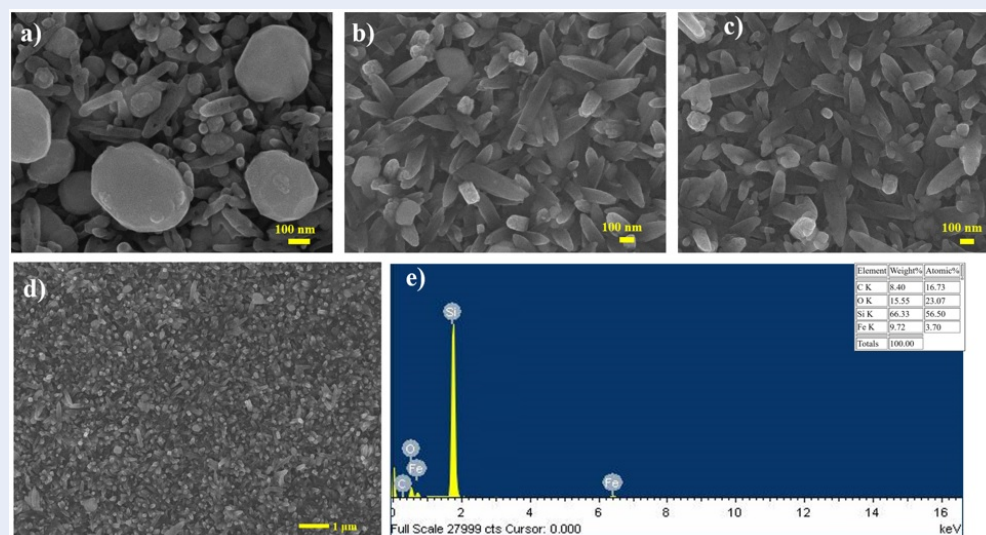


Figure 4: SEM images of α -Fe₂O₃ NRs at different hydrothermal times: a) 3 h, b) 4 h, and c) 5 h. d) Large-scale SEM image and e) EDX spectrum of the α -Fe₂O₃ NRs sample after 4 h of hydrothermal treatment.

241 the α phase of Fe₂O₃ with the depicted crystal structure. Additionally, the fundamental parameters of the
 242 structure. Additionally, the fundamental parameters of the
 243 diffraction peaks obtained from the simulation are clearly depicted in Table 1. In the UV-Vis absorption
 244 spectrum (Figure 3), the α -Fe₂O₃ NRs exhibit a wide absorption range, with a peak at a wavelength
 245 of approximately 400 nm. The optical band gap was calculated at a value of 2.2 eV using Tauc's method.
 246 This indicates the suitability of α -Fe₂O₃ NRs for efficient photocatalytic applications under visible light.
 247 In addition, nanorods subjected to 4 hours of hydrothermal treatment exhibited uniform growth with
 248 high density, with an average diameter of 110 nm and

254 a length of 415 nm (depicted in Figure 4b and Figure
 255 4d). Additionally, the EDX spectrum (Figure 4e)
 256 only detected the presence of elements that make up
 257 hematite (Fe and O), along with signals from the silicon
 258 substrate (Si) and carbon tape (C) utilized during the
 259 EDX measurement process. This further underscores the
 260 high purity of the prepared sample. Therefore, α -Fe₂O₃ NRs present distinct advantages for applications
 261 requiring large surface areas or structured patterns, particularly in the realm of photocatalysis,
 262 due to their exceptional adsorption capacity for decomposing organic compounds. In the Raman spectrum
 263 of α -Fe₂O₃ depicted in Figure 5, the peaks cor-
 264
 265
 266

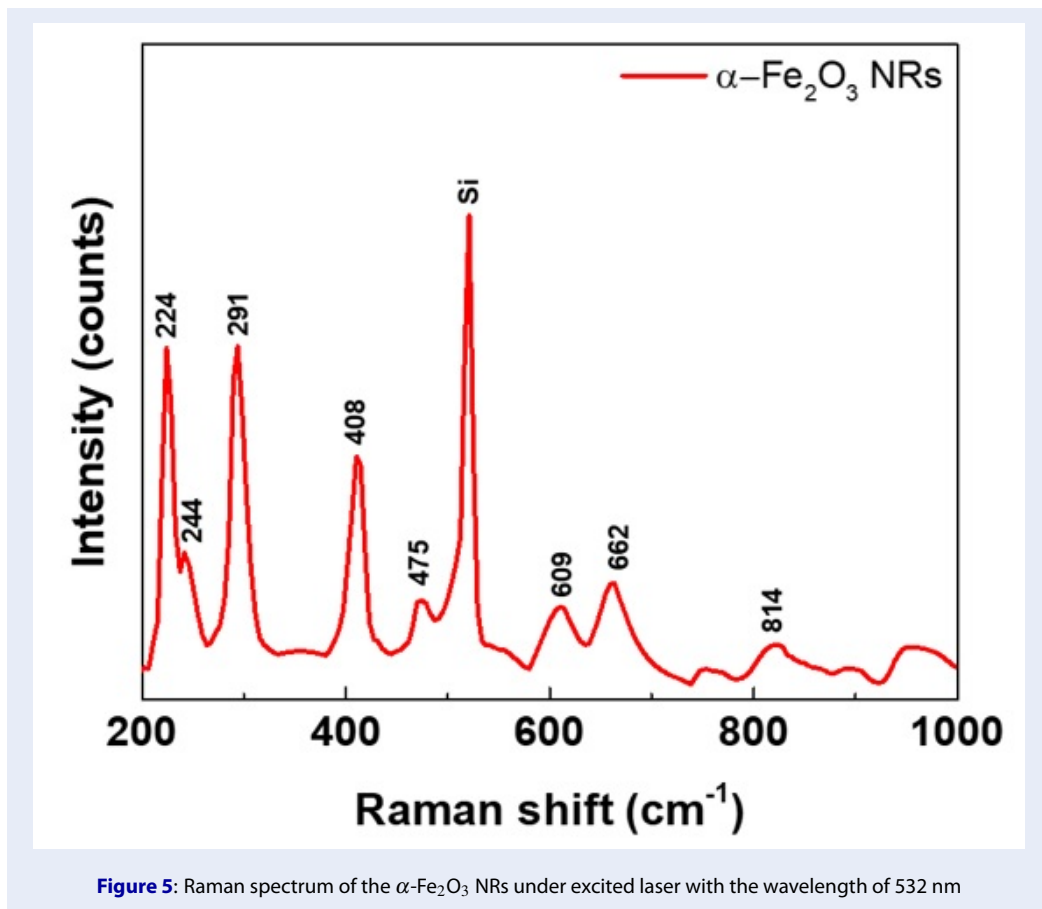


Figure 5: Raman spectrum of the $\alpha\text{-Fe}_2\text{O}_3$ NRs under excited laser with the wavelength of 532 nm

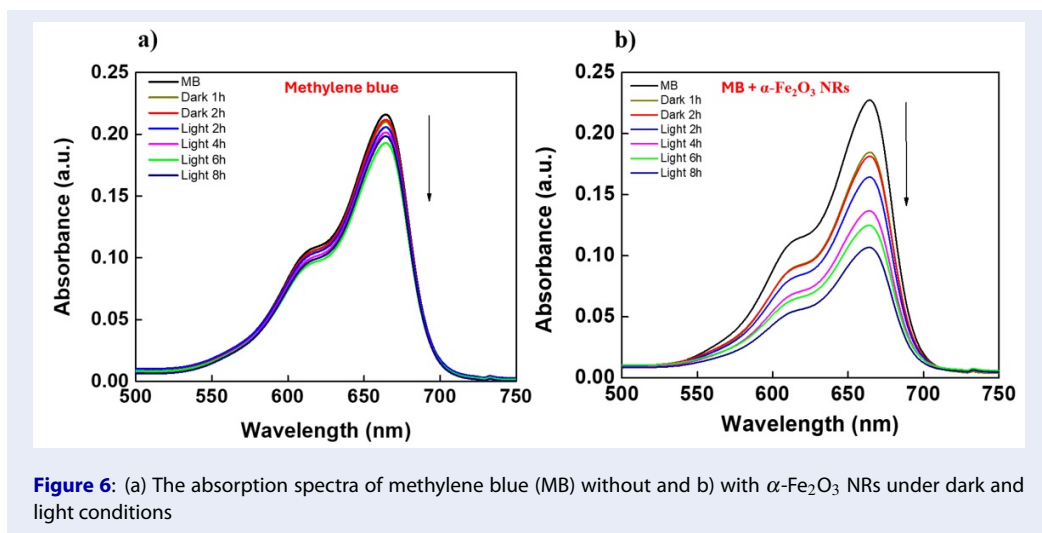


Figure 6: (a) The absorption spectra of methylene blue (MB) without and b) with $\alpha\text{-Fe}_2\text{O}_3$ NRs under dark and light conditions

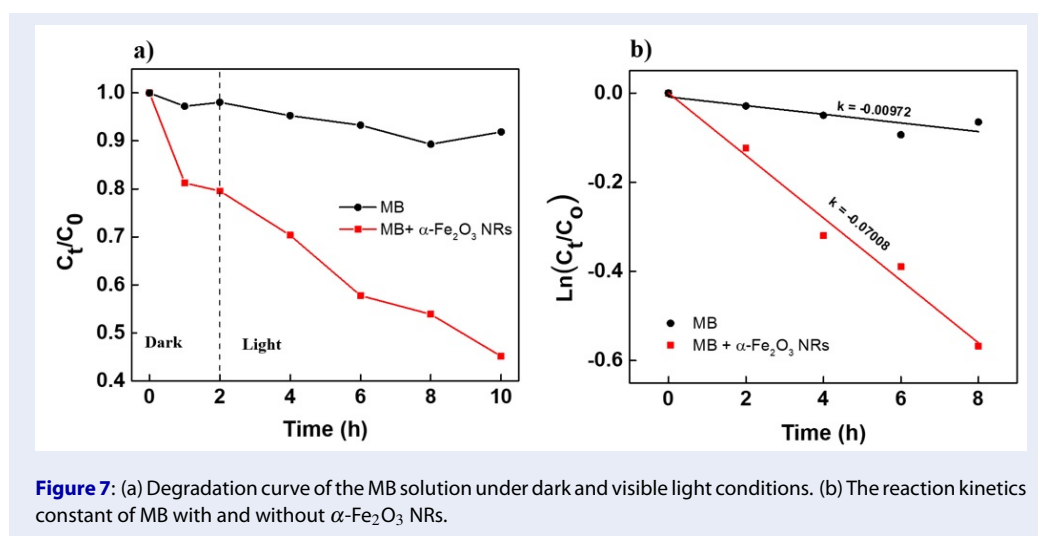


Figure 7: (a) Degradation curve of the MB solution under dark and visible light conditions. (b) The reaction kinetics constant of MB with and without α -Fe₂O₃ NRs.

267 responding to the A_{1g} vibrational mode at 224 and
 268 475 cm^{-1} indicate symmetric stretching vibrations of
 269 the Fe–O bond, while those assigned to the E_g mode at
 270 244, 291, 408, 609, and 814 cm^{-1} represent symmetric
 271 bending vibrations of the same bond⁷. Besides,
 272 the characteristic peaks of hematite mentioned above,
 273 the appearance of vibrations at around 662 cm^{-1} is
 274 related to larger nanoparticles than to the size of the
 275 nanostructured particles^{8,9}. This may explain why
 276 this peak is not always observed in the Raman spectra
 277 of nanostructured hematite¹⁰. This result is consistent
 278 with the SEM images demonstrating the synthesis
 279 of α -Fe₂O₃ as nanorods. Moreover, the detected
 280 Raman bands signify the propagation of lattice vibration
 281 waves, known as phonons, arising from repetitive
 282 and systematic oscillations of the crystal lattice within
 283 the hematite structure¹¹. Notably, the characteristic
 284 vibration peaks of hematite synthesized through this
 285 method exhibit high sharpness and clarity. Comparing
 286 the Raman spectrum with the XRD pattern (Figure 2)
 287 reaffirms the high crystallization of the synthesized
 288 hematite structure. Furthermore, apart from the silicon
 289 substrate peak at 521 cm^{-1} , no anomalous peaks
 290 indicative of parasitic phases, other iron oxides,
 291 or iron oxyhydroxides were detected. Moreover, the
 292 dye degradation efficiency was calculated using the
 293 following equation¹²:

$$294 \text{ \% dye degradation} = [(C_0 - C_t) / C_0] \times 100\% \quad (1)$$

295 The photodegradation of these nanomaterials was
 296 also quantitatively described using the pseudo-first-
 297 order kinetic equation, which is the most common
 298 rate law and was adopted as follows¹³:

$$299 \ln(C_t / C_0) = -kt \quad (2)$$

300 where C_0 and C_t are the initial dye concentration and
 301 dye concentration at time 't', respectively.

The results indicate that in the absence of a catalyst, 302
 the self-degradation capacity of MB (2.5 ppm) is only 303
 approximately 10%. With the α -Fe₂O₃ NRs catalyst 304
 in the MB sample, after adsorption-desorption equi- 305
 librium, the MB concentration decreased to 78% of 306
 the initial concentration. This reduction corresponds 307
 to the removal of approximately 22% of MB due to its 308
 absorption onto the material's surface. After 8 h of 309
 the photocatalytic reaction, the MB concentration de- 310
 creased further to 45%, indicating an additional 33% 311
 removal through the photocatalytic process. These re- 312
 sults demonstrate that 55% of the α -Fe₂O₃ NRs were 313
 removed in this study. Furthermore, the reaction rate 314
 constant of the MB solution in the presence of the 315
 α -Fe₂O₃ NRs catalyst is -0.07008, approximately 7.2 316
 times greater than the rate constant of MB without α - 317
 Fe_2O_3 NRs, which is -0.00972. Although the photo- 318
 catalytic efficiency of α -Fe₂O₃ NRs is not yet high, 319
 this material has potential due to the simplicity of the 320
 fabrication process and sample recovery after the cat- 321
 alytic reaction. 322

323 CONCLUSIONS

In summary, we have successfully synthesized α - 324
 Fe_2O_3 nanorods through a simple, rapid, and cost- 325
 effective process, yielding promising results. Specifi- 326
 cally, nanorods with average lengths and diameters 327
 of 415 nm and 110 nm, respectively, were grown 328
 at a uniform density. Furthermore, the synthesized 329
 nanorods exhibited an E_g of 2.2 eV and demon- 330
 strated a 55% degradation efficiency of MB through- 331
 out the entire process. Additionally, through a com- 332
 bination of experimental and simulation approaches, 333
 it has been confirmed that these α -Fe₂O₃ nanorods 334

Table 1: Basic parameters of the diffraction peaks of α -Fe₂O₃

h	k	l	2 θ	d (Å)	h	k	l	2 θ	d (Å)
0	1	2	23.942	3.7137	2	1	10	93.019	1.0618
1	0	4	32.976	2.7141	4	0	4	94.388	1.0499
1	1	0	35.223	2.546	1	1	12	94.805	1.0464
0	0	6	39.21	2.2957	1	3	7	95.73	1.0387
1	1	3	40.481	2.2266	3	2	1	99.542	1.0089
2	0	2	43.04	2.0999	1	2	11	100.6	1.0011
0	2	4	49.019	1.8569	2	3	2	100.63	1.0009
1	1	6	53.719	1.7049	3	1	8	101.17	0.9971
2	1	1	55.49	1.6546	2	2	9	103.83	0.9787
1	2	2	56.784	1.62	3	2	4	105.05	0.9706
0	1	8	57.407	1.6039	4	1	0	106.35	0.9623
2	1	4	61.788	1.5002	0	1	14	106.68	0.9603
3	0	0	63.208	1.4699	2	3	5	108.41	0.9497
1	2	5	65.39	1.426	1	4	3	109.75	0.9418
2	0	8	69.17	1.357	4	1	3	109.75	0.9418
1	0	10	71.73	1.3148	0	4	8	112.13	0.9284
1	1	9	71.923	1.3117	1	3	10	114.76	0.9146
2	2	0	74.474	1.273	3	0	12	116.74	0.9047
2	1	7	74.554	1.2718	0	3	12	116.74	0.9047
3	0	6	76.963	1.2379	3	2	7	117.77	0.8997
0	3	6	76.963	1.2379	2	0	14	118.04	0.8985
2	2	3	77.797	1.2267	2	1	13	118.96	0.8942
1	3	1	78.44	1.2182	4	1	6	120.45	0.8875
3	1	2	79.536	1.2042	1	4	6	120.45	0.8875
1	2	8	80.066	1.1975	3	1	11	123.38	0.8749
0	2	10	82.506	1.1682	5	0	2	123.42	0.8748
1	3	4	83.882	1.1525	2	3	8	124.04	0.8722
0	0	12	84.3	1.1479	1	1	15	126.18	0.8638
3	1	5	87.118	1.1178	4	0	10	127.01	0.8607
2	2	6	87.564	1.1133	0	5	4	128.74	0.8544
0	4	2	90.083	1.0886					

335 possess a rhombohedral crystal structure and belong
 336 to the space group $R\bar{3}c$. With this characterization,
 337 we hope to provide valuable insights to facilitate fur-
 338 ther research endeavors based on α -Fe₂O₃ nanorods,
 339 thereby expanding the potential applications of this
 340 material in the future.

341 **COMPETING INTERESTS**

342 The authors declare that there are no conflicts of in-
 343 terest related to the publication of this article.

344 **AUTHORS' CONTRIBUTIONS**

345 **H. N. Luong:** carried out the experiment, writing
 346 manuscript. **H. N. Luong, L. T. Duy:** measured and
 347 analyzed XRD data based on experiments and simu-
 348 lations. **L. N. T. Nguyen, C. K. Tran:** measured, an-
 349 alyzed SEM and UV-Vis data. **H. N. Luong, T. M.**
 350 **Dinh, N. D. N. Huynh:** investigated the material's
 351 capacity for degrading MB via the photocatalytic pro-
 352 cess.. **V. Q. Dang:** managed the experiment, collected
 353 data to write the paper.

354 **ACKNOWLEDGMENTS**

355 This research is funded by Vietnam National Foun-
 356 dation for Science and Technology Development
 357 (NAFOSTED) under grant number 103.03-2021.59.

358 **REFERENCES**

359 1. Iijima S. Helical microtubules of graphitic carbon. *Nature* 1991;
 360 354: 56-58; Available from: <https://doi.org/10.1038/354056a0>.
 361 2. Hsu C-Y, Rheima AM, Abbas Z sabri, Faryad MU, Kadhim MM,
 362 Altimari US et al. Nanowires Properties and Applications: A
 363 Review Study. *South African Journal of Chemical Engineer-*
 364 *ing* 2023; 46: 286-311; Available from: [https://doi.org/10.1016/](https://doi.org/10.1016/j.sajce.2023.08.006)
 365 [j.sajce.2023.08.006](https://doi.org/10.1016/j.sajce.2023.08.006).
 366 3. Abdullah M, Kamarudin SK. Titanium dioxide nanotubes (TNT)
 367 in energy and environmental applications: An overview. *Ren-*
 368 *ewable and Sustainable Energy Reviews* 2017; 76: 212-
 369 225; Available from: <https://doi.org/10.1016/j.rser.2017.01.057>.
 370 4. Naidu KCB, Kumar NS, Banerjee P, Reddy BVS. A review on the
 371 origin of nanofibers/nanorods structures and applications. *J*
 372 *Mater Sci: Mater Med* 2021; 32: 68; PMID: 34117944. Available
 373 from: <https://doi.org/10.1007/s10856-021-06541-7>.
 374 5. Sharmin M, Podder J. Band gap tuning, n-type to p-type tran-
 375 sition and ferrimagnetic properties of Mg doped α -Fe₂O₃
 376 nanostructured thin films. *Journal of Alloys and Compounds*
 377 2020; 818: 152850; Available from: [https://doi.org/10.1016/j.](https://doi.org/10.1016/j.jallcom.2019.152850)
 378 [jallcom.2019.152850](https://doi.org/10.1016/j.jallcom.2019.152850).
 379 6. Arun T, Prabakaran K, Udayabhaskar R, Mangalaraja RV,
 380 Akbari-Fakhrabadi A. Carbon decorated octahedral shaped
 381 Fe₃O₄ and α -Fe₂O₃ magnetic hybrid nanomaterials for next
 382 generation supercapacitor applications. *Applied Surface Sci-*
 383 *ence* 2019; 485: 147-157; Available from: [https://doi.org/10.](https://doi.org/10.1016/j.apsusc.2019.04.177)
 384 [apsusc.2019.04.177](https://doi.org/10.1016/j.apsusc.2019.04.177).
 385 7. Tadic M, Kopanja L, Panjan M, Lazovic J, Tadic BV, Stanoje-
 386 vic B et al. Rhombohedron and plate-like hematite (α -Fe₂O₃)
 387 nanoparticles: synthesis, structure, morphology, magnetic
 388 properties and potential biomedical applications for MRI. *Ma-*
 389 *terials Research Bulletin* 2021; 133: 111055; Available from:
 390 <https://doi.org/10.1016/j.materresbull.2020.111055>.

8. Wang X, Wang T, Si G, Li Y, Zhang S, Deng X et al. Oxygen
 391 vacancy defects engineering on Ce-doped α -Fe₂O₃ gas sen-
 392 sor for reducing gases. *Sensors and Actuators B: Chemical*
 393 2020; 302: 127165; Available from: [https://doi.org/10.1016/j.](https://doi.org/10.1016/j.snb.2019.127165)
 394 [snb.2019.127165](https://doi.org/10.1016/j.snb.2019.127165).
 395 9. Lv X, Zheng P, Wu Z, Yu J, Ge D, Yang L. Self-assembly of
 396 Fe₂O₃ nanorods in carbon nanotube network as a 3D aerogel
 397 architecture for lithium-ion batteries. *Ceramics International*
 398 2019; 45: 5796-5800; Available from: [https://doi.org/10.1016/j.](https://doi.org/10.1016/j.ceramint.2018.12.047)
 399 [ceramint.2018.12.047](https://doi.org/10.1016/j.ceramint.2018.12.047).
 400 10. Gerami SE, Pourmadadi M, Fatoorehchi H, Yazdian F,
 401 Rashedi H, Nigjeh MN. Preparation of pH-sensitive
 402 chitosan/polyvinylpyrrolidone/ α -Fe₂O₃ nanocomposite
 403 for drug delivery application: Emphasis on ameliorating
 404 restrictions. *International Journal of Biological Macro-*
 405 *molecules* 2021; 173: 409-420; PMID: 33454326. Available
 406 from: <https://doi.org/10.1016/j.ijbiomac.2021.01.067>.
 407 11. Xiao C, Li J, Zhang G. Synthesis of stable burger-like α -Fe₂O₃
 408 catalysts: Formation mechanism and excellent photoFenton
 409 catalytic performance. *Journal of Cleaner Production* 2018;
 410 180: 550-559; Available from: [https://doi.org/10.1016/j.jclepro.](https://doi.org/10.1016/j.jclepro.2018.01.127)
 411 [2018.01.127](https://doi.org/10.1016/j.jclepro.2018.01.127).
 412 12. Alhabrabi M, Nundy S, Ghosh A, Tahir AA. Vertically Aligned
 413 CdO-Decked α -Fe₂O₃ Nanorod Arrays by a Radio Frequency
 414 Sputtering Method for Enhanced Photocatalytic Applications.
 415 *ACS Omega* 2022; 7: 28396-28407; PMID: 35990474. Available
 416 from: <https://doi.org/10.1021/acsomega.2c02996>.
 417 13. Popov N, Krehula S, Ristić M, Kuzmann E, Homonnay Z,
 418 Bošković M et al. Influence of Cr doping on the structural,
 419 magnetic, optical and photocatalytic properties of α -Fe₂O₃
 420 nanorods. *Journal of Physics and Chemistry of Solids* 2021;
 421 148: 109699; Available from: [https://doi.org/10.1016/j.jpcs.](https://doi.org/10.1016/j.jpcs.2020.109699)
 422 [2020.109699](https://doi.org/10.1016/j.jpcs.2020.109699).
 423 14. Yan X, Wu Y, Li D, Hu J, Li G, Li P et al. Synthesis and evolution
 424 of α -Fe₂O₃ nanorods for enhanced visible-light-driven pho-
 425 to catalysis. *J Mater Sci* 2018; 53: 15850-15858; Available from:
 426 <https://doi.org/10.1007/s10853-018-2751-0>.
 427 15. Demirci S, Yurdaskal M, Dikici T, Sarıoğlu C. Fabrication
 428 and characterization of novel iodine doped hollow and
 429 mesoporous hematite (Fe₂O₃) particles derived from sol-gel
 430 method and their photocatalytic performances. *Journal of*
 431 *Hazardous Materials* 2018; 345: 27-37; PMID: 29128724. Avail-
 432 able from: <https://doi.org/10.1016/j.jhazmat.2017.11.009>.
 433 16. Tadic M, Trpkov D, Kopanja L, Vojnovic S, Panjan M. Hydrother-
 434 mal synthesis of hematite (α -Fe₂O₃) nanoparticle forms: Syn-
 435 thesis conditions, structure, particle shape analysis, cytotox-
 436 icity and magnetic properties. *Journal of Alloys and Com-*
 437 *pounds* 2019; 792: 599-609; Available from: [https://doi.org/10.](https://doi.org/10.1016/j.jallcom.2019.03.414)
 438 [1016/j.jallcom.2019.03.414](https://doi.org/10.1016/j.jallcom.2019.03.414).
 439 17. Wu M-S, Ou Y-H, Lin Y-P. Iron Oxide Nanosheets and Nanopar-
 440 ticles Synthesized by a Facile Single-Step Coprecipitation
 441 Method for Lithium-Ion Batteries. *J Electrochem Soc* 2011;
 442 158: A231; Available from: <https://doi.org/10.1149/1.3527982>.
 443 18. Khalil AT, Ovais M, Ullah I, Ali M, Shinwari ZK, Maaza M. Biosyn-
 444 thesis of iron oxide (Fe₂O₃) nanoparticles via aqueous ex-
 445 tracts of Sageretia thea (Osbeck.) and their pharmacognos-
 446 tic properties. *Green Chemistry Letters and Reviews* 2017;
 447 10: 186-201; Available from: [https://doi.org/10.1080/17518253.](https://doi.org/10.1080/17518253.2017.1339831)
 448 [2017.1339831](https://doi.org/10.1080/17518253.2017.1339831).
 449 19. Ramesh R, Ashok K, Bhalero GM, Ponnusamy S,
 450 Muthamizhchelvan C. Synthesis and properties of α -Fe₂O₃
 451 nanorods. *Crystal Research and Technology* 2010; 45: 965-
 452 968; Available from: <https://doi.org/10.1002/crat.201000140>.
 453 20. Pradhan GK, Parida KM. Fabrication, Growth Mechanism, and
 454 Characterization of α -Fe₂O₃ Nanorods. *ACS Appl Mater Inter-*
 455 *faces* 2011; 3: 317-323; PMID: 21214197. Available from:
 456 <https://doi.org/10.1021/am100944b>.
 457 21. Zeng S, Tang K, Li T. Controlled synthesis of α -Fe₂O₃ nanorods
 458 and its size-dependent optical absorption, electrochemical,
 459 and magnetic properties. *Journal of Colloid and Interface Sci-*
 460 *ence* 2007; 312: 513-521; PMID: 17498731. Available from:
 461

- 462 <https://doi.org/10.1016/j.jcis.2007.03.046>.
- 463 22. Zhang G-Y, Feng Y, Xu Y-Y, Gao D-Z, Sun Y-Q. Controlled
464 synthesis of mesoporous α -Fe₂O₃ nanorods and visible
465 light photocatalytic property. *Materials Research Bulletin*
466 2012; 47: 625-630; Available from: <https://doi.org/10.1016/j.materresbull.2011.12.032>.
- 467 23. Shi Y, Li H, Wang L, Shen W, Chen H. Novel α -
468 Fe₂O₃/CdS Corelike Nanorods with Enhanced Pho-
469 to-catalytic Performance. *ACS Appl Mater Interfaces*
470 2012; 4: 4800-4806; PMID: 22894770. Available from:
471 <https://doi.org/10.1021/am3011516>.
- 472 24. Pradhan GK, Padhi DK, Parida KM. Fabrication of α -Fe₂O₃
473 Nanorod/RGO Composite: A Novel Hybrid Photocatalyst for
474 Phenol Degradation. *ACS Appl Mater Interfaces* 2013; 5: 9101-
475 9110; PMID: 23962068. Available from: <https://doi.org/10.1021/am402487h>.
- 476 25. Chen D, Liu Z. Dual-Axial Gradient Doping (Zr and Sn) on
477 Hematite for Promoting Charge Separation in Photoelectro-
478 chemical Water Splitting. *ChemSusChem* 2018; 11: 3438-
479 3448; PMID: 30098118. Available from: <https://doi.org/10.1002/cssc.201801614>.
- 480 26. Dzade NY, Roldan A, De Leeuw NH. A Density Functional
481 Theory Study of the Adsorption of Benzene on Hematite (α -
482 Fe₂O₃) Surfaces. *Minerals* 2014; 4: 89-115; Available from:
483 <https://doi.org/10.3390/min4010089>.
- 484 27. Gedamu Tamirat A, Rick J, Aregahegn Dubale A, Su W-N,
485 Hwang B-J. Using hematite for photoelectrochemical wa-
486 ter splitting: a review of current progress and challenges.
487 *Nanoscale Horizons* 2016; 1: 243-267; PMID: 32260645. Avail-
488 able from: <https://doi.org/10.1039/C5NH00098J>.
- 489 28. Rao X, Su X, Yang C, Wang J, Zhen X, Ling D. From spindle-
490 like β -FeOOH nanoparticles to α -Fe₂O₃ polyhedral crystals:
491 shape evolution, growth mechanism and gas sensing prop-
492 erty. *CrystEngComm* 2013; 15: 7250-7256; Available from:
493 <https://doi.org/10.1039/c3ce40430g>.
- 494 29. Li F, Li J, Zhang J, Gao L, Long X, Hu Y et al. NiO Nanoparti-
495 cles Anchored on Phosphorus-Doped α -Fe₂O₃ Nanoarrays:
496 An Efficient Hole Extraction p-n Heterojunction Photoan-
497 ode for Water Oxidation. *ChemSusChem* 2018; 11: 2156-
498 2164; PMID: 29768719. Available from: <https://doi.org/10.1002/cssc.201800571>.
- 499 30. Su J, Feng X, Sloppy JD, Guo L, Grimes CA. Vertically Aligned
500 WO₃ Nanowire Arrays Grown Directly on Transparent Con-
501 ducting Oxide Coated Glass: Synthesis and Photoelectro-
502 chemical Properties. *Nano Lett* 2011; 11: 203-208; PMID:
503 21114333. Available from: <https://doi.org/10.1021/nl1034573>.
- 504 31. Wei Q, Zhang Z, Li Z, Zhou Q, Zhu Y. Enhanced photocat-
505 alytic activity of porous α -Fe₂O₃ films prepared by rapid ther-
506 mal oxidation. *J Phys D: Appl Phys* 2008; 41: 202002; Available
507 from: <https://doi.org/10.1088/0022-3727/41/20/202002>.
- 508 32. Bulin C, Li B, Zhang Y, Zhang B. Removal performance and
509 mechanism of nano α -Fe₂O₃/graphene oxide on aqueous
510 Cr(VI). *Journal of Physics and Chemistry of Solids* 2020;
511 147: 109659; Available from: <https://doi.org/10.1016/j.jpcs.2020.109659>.
- 512 33. Naveas N, Pulido R, Marini C, Hernández-Montelongo J, Sil-
513 ván MM. First-principles calculations of hematite (α -Fe₂O₃)
514 by self-consistent DFT+U+V. *iScience* 2023; 26: 106033; PMID:
515 36824287. Available from: <https://doi.org/10.1016/j.isci.2023.106033>.
- 516 517 518 519 520 521